Comparison of physics-based and machine learning methods for phase-resolved prediction of waves measured in the field

Jialun Chen, Thobani Hlophe, Wenhua Zhao, Ian A. Milne, David Gunawan, Adi Kurniawan, Hugh Wolgamot, Paul H. Taylor, and Jana Orszaghova

Abstract—**Phase-resolved predictions of surface waves can be used to optimize a wide variety of marine applications. In this paper, we compare predictions obtained using two independent methods for field data, with horizons sufficient to control wave energy converters.**

The first method is physics-based prediction. In this method, a set of optimal representative angles, obtained using an optimization algorithm given time histories of a wave buoy motion in 3D, are used for forward propagation based on linear wave theory. The second method is a machine learning method using an Artificial Neural Network (ANN) which requires longer records for training.

Field measurements were obtained from the Southern Ocean of Albany, WA. The field data were collected by an upwave 'detection' array of 3 Sofar Spotter wave buoys and a downwave 'prediction' point coincident with a Datawell Waverider-4. All buoys were soft-moored, and data were collected over 3 months in 2022. Selected intervals during this period are presented in the paper to compare and contrast the predictions made by the two different methods. We find that some wave fields can be predicted well over more than a period in advance, all that is required for active control of a power take-off in a wave energy application. In contrast, highly spread sea states remain a challenge. The methods are also compared in terms of the complexity and time required for making predictions. Further discussions are made on the applicability of the results to other locations.

Index Terms—**Wave prediction, Machine learning, Wave buoys, Field data, Wave phase, Control.**

I. Introduction

REAL-TIME phase-resolved wave prediction is highly desirable to ensure the safety and efficiency o f v arious o ffshore o perations. T he present study is motivated by the potential of wave prediction to enhance the economic viability of wave energy converters (WECs). Previous studies have demonstrated that a dramatic increase in power output can be achieved by actively controlled WECs [1], [2]. In [3], it is shown that accurate wave prediction of up to two wave periods is of great importance for WEC control—beyond that, the benefit does not justify the complexity of wave prediction. Additionally, large ocean waves pose a serious threat to WECs as they operate remotely in all various weather conditions, including during severe storms. Prediction of incoming waves could help ensure their survival and increase their lifespan.

Although the desired quality of predictions is application-specific, WEC control is expected to require prediction of the highest quality. However, accurate wave predictions are challenging to obtain, especially in the field, due to large directional wave spreading, which can result from swells coming from different storm sources, and local refraction due to sea-bed topography. Even with a large number of wave records, the many directional components comprising the wave field make it difficult to extract information on the initial phase shifts, required to accurately reconstruct the wave field at local spatial locations based on a finite number of plane waves.

Given the complexity presented by large wave spreading, there is a handful of research papers discussing highly spread waves, typical of real ocean waves. One of the few physics-based models is the optimized algebraic model of Hlophe et al. [4] based on the fast Fourier transform (FFT). The algebraic model, which is a novel development of the work [5], forms the basis of one of the methods compared here. The algebraic model was shown to be capable of achieving highly accurate predictions using 9 input records from sea states with spreading angles $\sigma_\theta \leq 25°$, where σ_θ is the standard deviation of a normal distribution used to describe wave propagation. Similar to the scheme of Fisher et al. [6], also validated using real ocean waves, the present algebraic model exploits all three degrees of freedom (DoF) translational displacements of each buoy: one vertically and two horizontally along the cardinal north and east. This significantly simplifies the deployment process that would be required with heave-only buoys or sensors as used in [5], [7]. Furthermore, the model employs a single frequency-independent set of directions to represent wave propagation, following [7], though frequency-dependent spreading is allowed.

An alternative approach is a machine learning method based on an Artificial Neural Network (ANN) that can learn complex relationships between input and output data. Using synthetic unidirectional waves, it

J. Chen, T. Hlophe, W Zhao, I. A. Milne, J. Orszaghova, A. Kur-niawan, H. Wolgamot, and P. H. Taylor are in the Oceans Graduate School, The University of Western Australia, Perth, 6009, Western Australia, Australia (e-mail: jialun.chen@research.uwa.edu.au).

TH, JO, AK, HW, and PHT are also in Marine Energy Research Australia, Great Southern Marine Research Facility, Albany, 6330, Western Australia, Australia.

D. Gunawan is in the School of Mathematics and Applied Statis-tics, The University of Wollongong, Wollongong, 2522, New South Wales, Australia.

Digital Object Identifier: https://doi.org/10.36688/ewtec-2023-488

has been shown in [8] and [9] that ANN-based models can provide more accurate predictions over linear wave theory predictions. Further, Zhang et al. [10] applied Bayesian Neural Networks, which extend standard neural networks with Bayesian inference, to quantify prediction uncertainty using wave tank data. However, the capability of spreading waves using ANN-based models is unknown and requires further investigation.

In this work, we compare the two different approaches: the physics-based algebraic model developed by [4] that propagates optimal directional components from buoy measurements based on linear dispersion, and the ANN-based model which is trained using past records of buoy measurements. As demonstrated previously in [4], the algebraic model can achieve accurate prediction (with error $\mathcal{E}_{\mathcal{R}} \leq 0.1$) for approximately a few wave periods ahead with reasonably large spreading angles. To understand, at least partially, the difficulties with very large wave spreading angles, we explore the performance of ANN in spreading waves. This paper aims to show the advantages and limitations of using the machine learning method compared to the physics-based method based on synthetic and field data.

II. Directionally spread wave fields

Real-time wave prediction becomes particularly challenging when dealing with large directional spreading, as elucidated in [11] using a mathematical expression for the variance of a prediction. Additionally, field data inevitably includes variability in environmental conditions such as wind, tides, and currents that can affect the behaviour of the waves and the array shape. It is also subject to measurement and interpretation errors, which need to be carefully evaluated and accounted for in the analysis. Hence, the complexity of field wave data makes it more difficult to predict accurately compared to 'clean' synthetic wave data. This study considers both synthetic and field wave data to provide a comprehensive understanding of the performance of physics-based and ANN-based models under different scenarios. Synthetic data can be generated under controlled conditions, allowing for a systematic comparison of the performance of the models, while field wave data is essential for comparing the performance of the models under real-world conditions.

A. Synthetic waves

The synthetic wave field is generated from a 2D wave spectrum, given as a product of a frequency spectrum $S(\omega)$ and a directional spreading function $D(\omega, \theta)$, according to

$$S(\omega, \theta) = S(\omega) D(\omega, \theta)\,, \tag{1}$$

where ω is the angular frequency and θ is the plane-wave propagation direction. In this work, angular spreading is assumed as a frequency-independent wrapped normal distribution:

$$D(\theta) = \frac{\Omega}{\sigma_\theta \sqrt{2\pi}} \exp\left(-\frac{(\theta - \overline{\theta})^2}{2\sigma_\theta^2}\right), \tag{2}$$

where Ω is a constant used to ensure a total probability of one in the finite band of θ, $\overline{\theta}$ is the mean wave direction, and σ_θ is the standard deviation of the distribution representing the size of wave spreading. Here, we assume that the directional spreading is frequency-independent; however, in general, both $\overline{\theta}$ and σ_θ can be functions of frequency. We mention in passing that for the commonly used $\cos^{2s}\theta/2$ spreading function, the spreading parameter s is related to σ_θ (given in radians) in (2) through $s = 2/\sigma_\theta^2$.

The linear surface wave elevation $\eta(\mathbf{x}, t)$ (to be predicted in this work) can be represented with random amplitudes related to Eq. (1) using a double summation in frequency and direction [12]:

$$\eta(\mathbf{x}, t) = \sum_{j=1}^{N_\omega} \sum_{i=1}^{N_\theta} A_{ij} \cos\left(-\mathrm{i}(\mathbf{k}_{ij} \cdot \mathbf{x} - \omega_j t + \epsilon_{ij})\right), \tag{3}$$

where A_{ij} are the wave amplitudes for each component, t is time, ϵ_{ij} are the initial phase shifts, $\mathbf{x} = (x, y)$ is the position in the horizontal plane, $\mathbf{k}_{ij} = k_j(\cos\theta_i, \sin\theta_i)$ are the wavenumber vectors with components in the x and y directions, N_θ is the number of directional components and N_ω is the number of frequency components. The wavenumber, $k = |\mathbf{k}|$, is related to the wave frequency through the linear dispersion relation:

$$\omega^2 = gk \tanh(kd), \tag{4}$$

where g is gravitational acceleration and d is a constant water depth.

B. Field wave measurements

Wave data were collected from July 21, 2022, to October 16, 2022, in the Southern Ocean at Sandpatch, Albany, Western Australia, using 3 Sofar Spotter buoys and one Datawell Waverider-4 (DWR4) buoy (see Fig. 1). These recorded displacements in all three degrees of freedom: surface elevation and the horizontal components to the east and north. The Spotter is a 0.42 m diameter spherical buoy powered by solar panels, which measures waves at 2.50 Hz with the GPS position every minute, while the DWR4 has a 0.90 m diameter hull with a battery and electrical components that measure waves at 2.56 Hz with GPS position every 2$^{\mathrm{nd}}$ and 10$^{\mathrm{th}}$ minutes. The location of the deployment is approximately 1 km offshore in a water depth of 33 m and the buoys were anchored to the seafloor using conventional mooring. Fig. 2 depicts the watch circles and anchor positions (at the center of the circles) of the Spotters and DWR4. It is noted that the discrepancy in the size of watch circles is due to the different mooring systems used—the DWR4 was already deployed for oceanographic research purposes, while the three Spotters were specifically deployed for wave prediction. It is important to consider the potential impact of using different types of buoys on the quality and comparability of the wave data collected and to account for any potential biases or sources of error in data analysis. This will be discussed in Section IV-B. It should also be noted that the anchor of the

Spotter 1 was displaced by 10 m around September 15, and the DWR4 stopped recording at around 12:00 on August 26 until August 28. Although the reasons for these incidents are unknown, such occurrences are to be expected in the field.

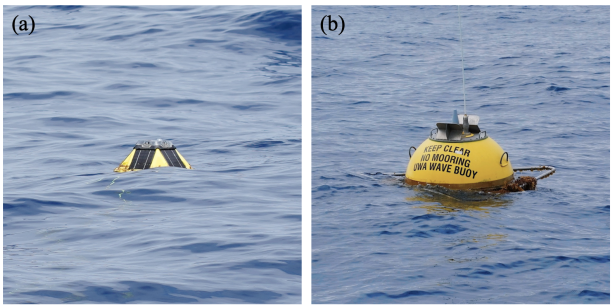

Fig. 1. (a) Sofar Spotter buoy, and (b) Datawell Waverider-4 (DWR4) buoy deployed in the Southern Ocean, near Albany, from 21 July to 16 October 2022.

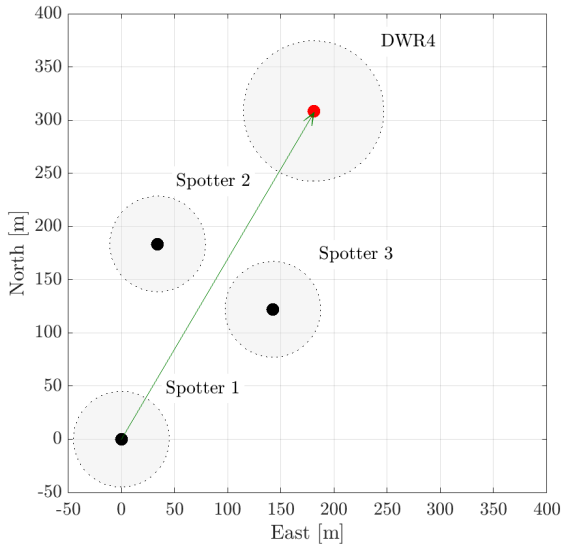

Fig. 2. Watch circles (dotted lines) and anchor positions of Spotters (black markers) and DWR4 (red marker). The green arrow denotes the average mean wave direction. The grey shading area represents the allowable range of movement restrained by the mooring line. The shoreline is roughly 1km north of the wave array and runs approximately East-southeast to west-northwest. The buoy array is aligned along the mean wave direction towards the north-northeast.

III. Methodology

This paper compares predictions obtained using the physics-based algebraic model in [4] and a machine learning model based on ANN. The algebraic model uses a set of optimal representative angles derived from the time histories of wave buoy motion, which are then used for forward propagation based on linear wave theory.In contrast, the ANN-based model is trained on the longer record of field data to learn and capture the complex relationships between upwave and downwave buoy motions without relying on any hydrodynamic equations or assumptions. By comparing these two models, we aim to gain valuable insights into the advantages and limitations of physics-based and ANN-based models, aiding in their further development for practical applications.

A. The algebraic model

The linear prediction model is fully presented in [4]. To reconstruct a single-frequency component, the surface elevation is represented by the complex amplitude

$$\eta(\mathbf{x},\omega) = \sum_{i=1}^{M} \{A_i \exp(-\mathrm{i}\epsilon_i)\} [\exp(-\mathrm{i}\mathbf{k}_i \cdot \mathbf{x})], \quad (5)$$

while the two corresponding horizontal in-plane displacements are given by

$$\boldsymbol{\zeta}(\mathbf{x},\omega) = \sum_{i=1}^{M} \{A_i \exp(-\mathrm{i}\epsilon_i)\} \left[\frac{-\mathrm{i}g\mathbf{k}_i}{\omega^2} \exp(-\mathrm{i}\mathbf{k}_i \cdot \mathbf{x})\right], \quad (6)$$

where $M \sim 5$ is the number of representative angles ϑ_i used to describe wave propagation in the whole field, i.e. $\mathbf{k}_i = k(\cos\vartheta_i, \sin\vartheta_i)$. Note that we use the second argument t or ω on the left-hand side of the equations, e.g. Eqs. (3) and (5), to indicate their time- and frequency-domain representations, respectively.

The terms in square brackets ([•]) in Eqs. (5) and (6) refer to the buoy locations $\mathbf{x}$ and the representative angles ϑ_i, which are known beforehand. However, the terms in curly brackets ({•}) are unknown and need to be estimated. To accomplish this, we formulate an over-determined system of linear equations, for a small number of buoys N_b, of the usual form

$$\mathbf{A}\mathbf{p} = \mathbf{q}, \quad (7)$$

where $\mathbf{A}$ is a $(3N_b \times M)$ complex coefficient matrix, $\mathbf{p}$ is a $(\dim(\mathbf{p}) = M)$ vector containing the unknown complex amplitudes and $\mathbf{q}$ is a $(\dim(\mathbf{q}) = 3N_b)$ vector of the Fourier amplitudes of the concurrently measured records (the 3 arises from the 3 DoF per buoy). It is recommended that the condition $3N_b \geq M$ is always satisfied. The system can be solved using least-squares methods in a very straightforward way—we employ singular value decomposition (SVD) in this paper.

The array $\mathcal{A}3$ and sets of representative directions $\boldsymbol{\vartheta}$ were solved for in an extensive optimization process detailed in [4]. The optimization is based on the minimization of an objective function, which is the time-averaged prediction error, i.e. the average of the error (Eq. (10)), in the forecast zone, before the rapid rise in the curves (see Fig. 6). Sets comprised of 4 directions, $|\boldsymbol{\vartheta}| = 4$, are found to give more accurate predictions for $\sigma_\theta > 19°$, while 5 directions are preferred for less spreading [13]. Since we are analyzing the same data as [13], where the spreading exceeds 20°, we will use the symmetric and asymmetric sets of representative angles, denoted $\boldsymbol{\vartheta}_{\mathcal{A}3}$ and $\boldsymbol{\vartheta}^{\star}_{\mathcal{A}3}$, respectively, given by

$$\begin{aligned} \boldsymbol{\vartheta}_{\mathcal{A}3} &= \theta_{\mathcal{A}} + \{-1.535, -0.448, 0.448, 1.535\}\sigma_\theta \\ \boldsymbol{\vartheta}^{\star}_{\mathcal{A}3} &= \theta_{\mathcal{A}} + \{-1.539, -0.287, 0.294, 1.307\}\sigma_\theta, \end{aligned} \quad (8)$$

where $\theta_{\mathcal{A}}$ is the pointing direction of the array calculated from the positions of Spotter 1 and the DWR4.

The full model sequentially executes the following operations: (1) inputs ocean wave records of $N_b \times 3$ DoF, (2) computes the autocorrelation function and its time derivatives up to the third from a single surface elevation record, (3) extends the ends of each record using NewWave terms [14], (4) uses the FFT to obtain the complex amplitudes in $\mathbf{q}$ of Eq. (7) and solves the system via SVD, and finally (5) predicts the surface elevation at the location $\mathbf{x}_4$ of the DWR4 based on linear wave propagation and inverse FFT.

An extension of the algebraic model employs inverse variance weighting (IVW) to obtain a composite prediction from multiple sets of propagation directions. The inverse of the variance of a prediction determines the level of accuracy which can be used to infer the 'weight' of that particular prediction. It is straightforward to apply IVW on synthetic data compared to field data since the weights are estimated from the numerical error, which needs to be computed from multiple realizations in a controlled sea-state environment. Therefore, for numerical data used in this paper, we employ the IVW, while we use $\vartheta^{\star}_{A3}$ for field data as done in [13].

B. Artificial Neural Network model

An ANN model is a type of machine learning algorithm that is inspired by biological nervous systems. It is capable of approximating complex relationships between input values, denoted as X, and output values, denoted as Y. The objective of an ANN model is to identify the optimal approximation function $\mathcal{F}$, by learning the values of parameters W and b, where $Y = \mathcal{F}(X; W, b)$, with W denoting set of weights vector and b set of bias terms. See [15], [16] for more details.

A wave prediction scheme using an ANN model can be summarized into the following steps: (1) The wave record is split into 3 segments: training, validation, and testing data. The training data provide examples for learning and fitting the parameters (i.e., weights and biases) of the ANN model. (2) The validation data help to tune hyper-parameters (i.e., numbers of layers, neurons, learning rate), avoiding over-fitting and validating the effectiveness of the model. (3) The testing data evaluate the prediction performance after training. Note that the training and prediction scheme for synthetic and field data are applied independently.

The schematic of the training process is illustrated in Fig. 3. The time histories of the surface elevation and horizontal displacements (along the cardinal east and north) of the three Spotters at upwave locations are used as input to map the surface elevation at DWR4 downwave, using the approximation function $\mathcal{F}$. Consider three data streams (horizontal displacements ζ_x, ζ_y, and surface elevation η) measured by each Spotter, denoted by $S_i \in \{\zeta_x(\mathbf{x}_i, t), \zeta_y(\mathbf{x}_i, t), \eta(\mathbf{x}_i, t)\}$ for $i = 1, 2, 3$, where the subscript i denotes the Spotter index. The surface elevation of DWR4 at position $\mathbf{x}_4$ can be approximated by the function as

$$\eta(\mathbf{x}_4, t) = \mathcal{F}(S_1, S_2, S_3; W, b)\,. \tag{9}$$

We rearranged approximately 6 hours of training data into approximately 20000 sets using a sliding window technique with a sliding offset of 1 s. Each training set consists of 204.5 s of input and 264.5 s of output ($-204.5 \leq t \leq 0$ s for reconstruction and $0 < t \leq 60$ s for forecasting). The obtained predictions are compared with the target values using the loss function (here, mean square error). The model is optimized by updating the network parameters (i.e., weights and biases) iteratively until the loss function reaches a minimum or stopping criterion.

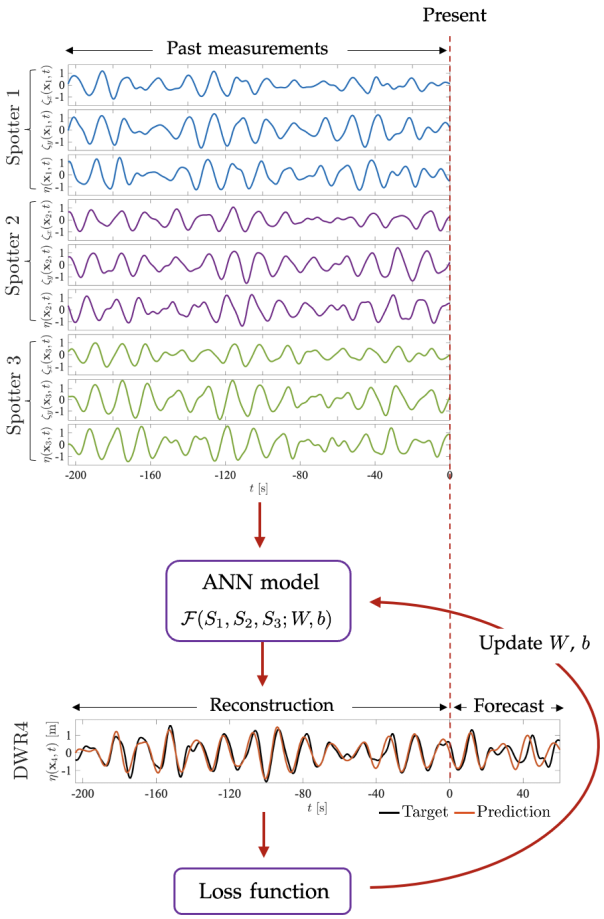

Fig. 3. Training process of the ANN model for wave prediction. The time history of surface wave elevation (η) and horizontal displacements ($\zeta_{x,y}$) of three Spotters at upwave locations are measured to map the surface wave elevation of DWR4 at the downwave location.

Based on sensitivity analysis, the ANN model is carried out using two hidden layers, each with 150 neurons. We select the rectified linear unit (ReLU) [17] as the activation function and Adam optimizer [18] as the gradient descent algorithm with the learning rate of 10^{-3} and a batch size of 128. An early stoppage is applied to stop the training process at a point when performance on a validation set decreases to prevent over-fitting. The ANN model is implemented in Python using the Keras [19] and Tensorflow [20] packages using a computer with an 8-core CPU, 14-core GPU, and 16GB RAM. The computation time for training takes approximately 5 minutes using the wave records from the past 6 hours, and predictions for the next hour are completed within a fraction of a second.

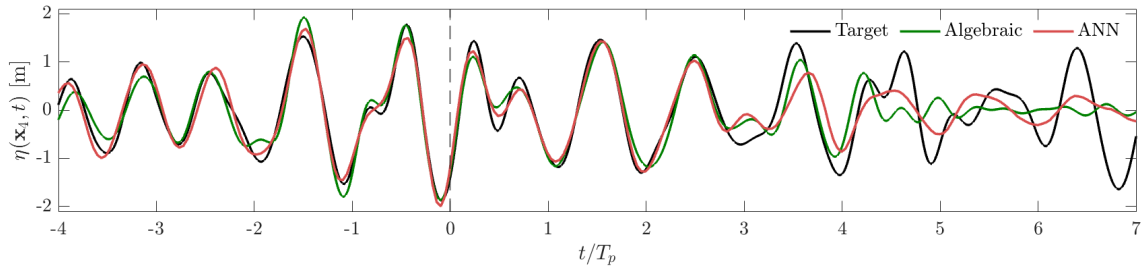

Fig. 4. Comparison of predictions from the algebraic and ANN models for a single realization from a synthetic sea state with spreading angle $\sigma_\theta = 20°$, and mean wave direction $\overline{\theta} = 0°$. The vertical dashed line divides the predicted output into reconstruction (past) and forecast (future).

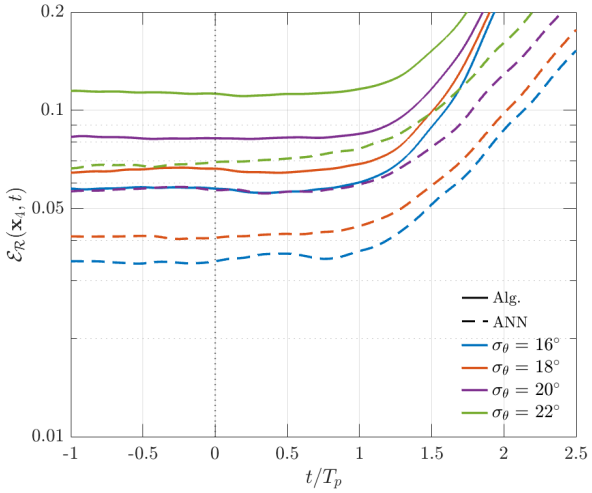

Fig. 5. Comparison of normalized error plot between the algebraic (solid line) and ANN (dashed line) models with mean wave direction $\overline{\theta} = 0°$, and varying spreading angle, σ_θ.

C. Error assessment

To compare the algebraic and ANN models, we quantify the prediction error between the target surface elevation η and the prediction $\tilde{\eta}$ using the normalized error given by

$$\mathcal{E}_\mathcal{R}(\mathbf{x}_4, t) = \frac{1}{\sigma^2 N_R} \sum_{i=1}^{N_R} (\eta_i(\mathbf{x}_4, t) - \tilde{\eta}_i(\mathbf{x}_4, t))^2 \quad , \qquad (10)$$

where σ^2 is the variance of the target surface elevation, and N_R is the number of realizations smoothed with a moving average.

IV. Comparison of Predictions from the Algebraic and ANN Models

A. Synthetic data

The synthetic linear, short-crested wave fields are generated with a JONSWAP spectrum with peak-enhancement factor $\gamma = 3.3$. We use a significant wave height $H_s = 3$ m, peak period $T_p = 12$ s, and water depth $d = 33$ m to represent the Albany location. The upper frequency of the energy spectrum is taken as $3\omega_p$, where ω_p is the peak angular frequency. The individual wave propagation directions ($N_\theta = 25$) from (2) are uniformly spaced within the interval $[-3\sigma_\theta + \overline{\theta}, 3\sigma_\theta + \overline{\theta}]$. All predictions in this study use input time histories of 204.5 s and 204.8 s duration (from Spotter 1, 2, and 3) as input for the ANN and algebraic models, respectively, to predict at DWR4. It should be noted that the sampling resolution for the ANN model is set to 0.5 s to reduce the computation time for training and decreasing the resolution further does not lead to improved accuracy, whereas the sampling resolution for the algebraic model is kept at 0.2 s, consistent with [4].

Figure 4 shows an example of the predictions from the algebraic and ANN models based on a random realization with spreading angle $\sigma_\theta = 20°$, and mean wave direction $\overline{\theta} = 0°$ using the array geometry in Fig. 2. At a glance, the ANN model shows a closer match with the target signal out to about $3T_p$ where both predictions start to break down completely. We now calculate the prediction error out of a large number (> 500) of realizations for different wave spreading: $\sigma_\theta \in [16, 22°]$. From Fig. 5, it is clear that the ANN model is superior to the algebraic model for these ideal simulations. Note that the error plots of the ANN model appear less smooth than the algebraic model due to the stochastic process of ANN model, which can introduce variability in the prediction results.

We then investigate the model performances with varying both the sea-state mean wave direction $\overline{\theta}$ and spreading angle σ_θ. Results are depicted by the contour plots in Fig. 6. It can be seen that the prediction performance of the algebraic model strongly depends on the size of the spreading and mean wave directions. In comparison, the ANN model is less dependent, with wider coverage in mean wave directions and better tolerance in spreading angles, indicating that a better match for the predictions to the target can be obtained. Specifically, the ANN model can achieve accurate prediction ($\mathcal{E}(t) \leq 0.1$) up to $1.5T_p$ for $\overline{\theta} = 0°$ with $\sigma_\theta \leq 22°$, while the algebraic model is constrained to $1.2T_p$ for $\overline{\theta} = 0°$ with $\sigma_\theta \leq 20°$. We note though that both models would appear to be adequate as input to WEC control.

While the above study demonstrates the effectiveness of ANN model for synthetic spread waves, it is worth noting that the ANN model is trained with specific wave conditions (i.e., H_s, T_p, σ_θ, and $\overline{\theta}$) and under the assumption that the locations of the wave buoys would remain constant. Hence, the consistency of wave conditions between the training and testing sets is ensured. The following section compares the two models from a practical point of view, using field data with varying wave conditions and slowly moving buoy

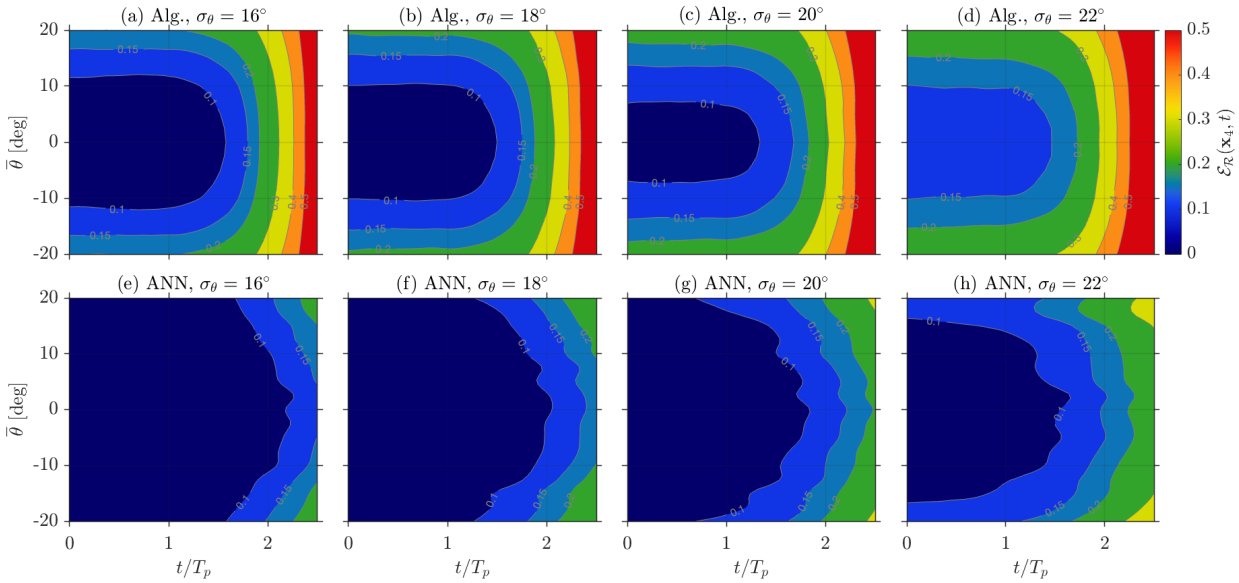

Fig. 6. Comparison of normalized prediction errors from the algebraic (top row) and ANN (bottom row) models with varying mean wave directions $\overline{\theta}$, and spreading angle σ_θ based on synthetic data.

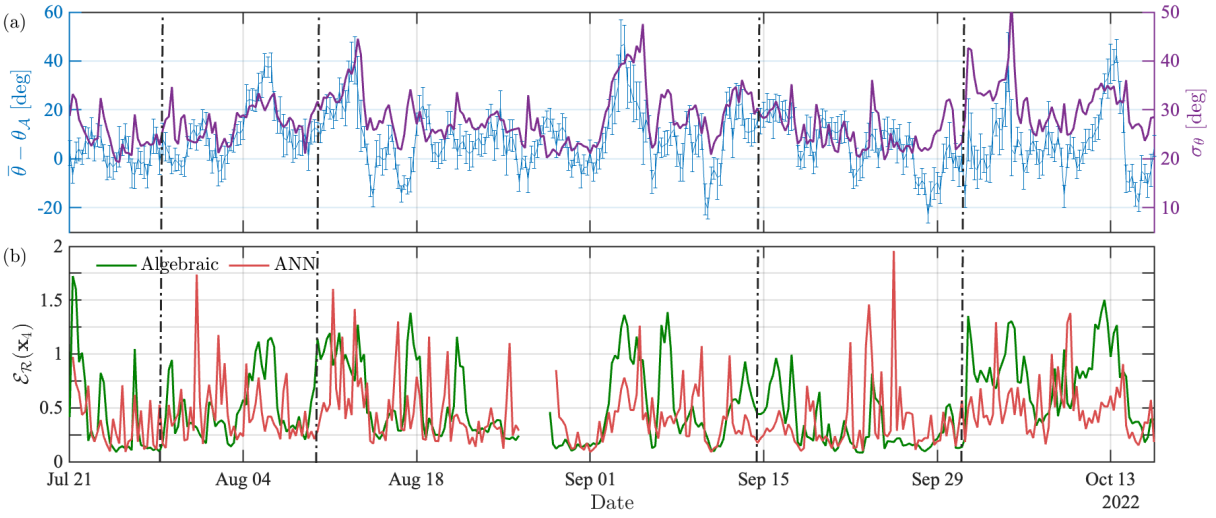

Fig. 7. Time-averaged prediction error over a horizon of 12 s for the first hour of every 6 hours. (a) Separation angles $\overline{\theta} - \theta_A$ and spreading angle σ_θ. (b) Comparison between the algebraic and ANN models.

positions.

B. Field data

The data set consists of samples taken every 6 hours over 88 days. Specifically, we compare the prediction results during the first hour of each 6-hour interval. Prior to prediction, the data are filtered using a band-pass over the linear range of frequencies, $[0.6\ 3.0]\omega_p$. Fig. 7(a) shows separation angles $\overline{\theta} - \theta_A$ with error bars that indicate the range of variation within an hour, where θ_A is the array pointing direction at a specific time, and $\overline{\theta}$ is the mean wave direction in the hour. The root-mean-square (RMS) spreading angle σ_θ (an averaged angle away from the mean wave direction) is plotted along the separation angles. The directional bulk parameters ($\overline{\theta}$, σ_θ) are derived from the Fourier coefficients [21] based on the 3-DoF records. Figure 7(b) shows the averaged prediction error over a horizon of 12 s within an hour using a 20 s moving window for both models. Note that there is no prediction between August 26 and August 28 due to the loss of data from the DWR4 during this interval. Moreover, in order to optimize the prediction performance for the next hour, the ANN model requires the past 6 hours of training data. As a result, the initial 6-hour period of the ANN model will also have no predictions.

In Fig. 7, it is evident that the prediction error using the algebraic model strongly depends on the separation and spreading angles, making it less reliable for larger angles. In contrast, the predictions from the ANN model are slightly less sensitive to these bulk parameters. We note that the ANN model has a better capability to predict waves with large spreading and separation angles, which is consistent with the synthetic results. Despite this, the ANN model exhibits numerous error spikes seen in Fig. 7(b), even when the algebraic model can achieve high accuracy. To

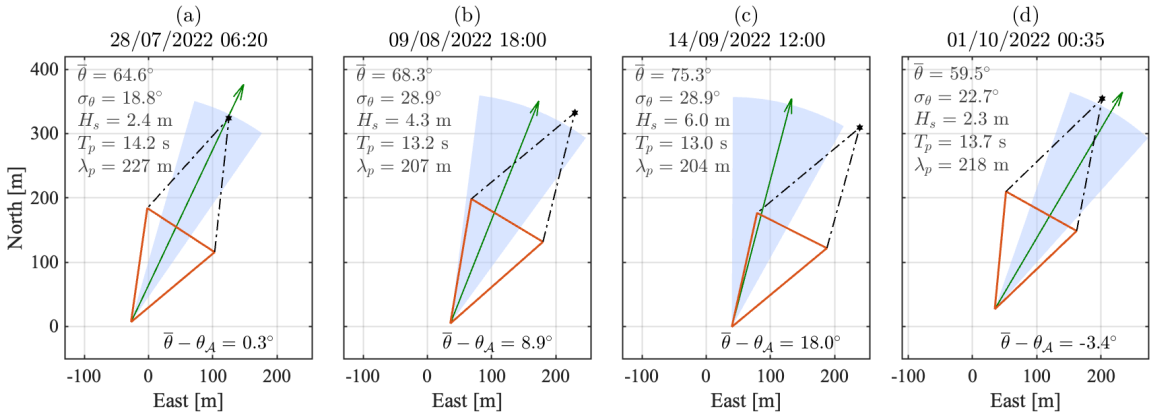

Fig. 8. Array positions correspond to the predictions in Fig. 9. The mean wave direction is indicated by green arrows ($2\lambda_p$ in length), and the blue shading area represents the wave spreading.

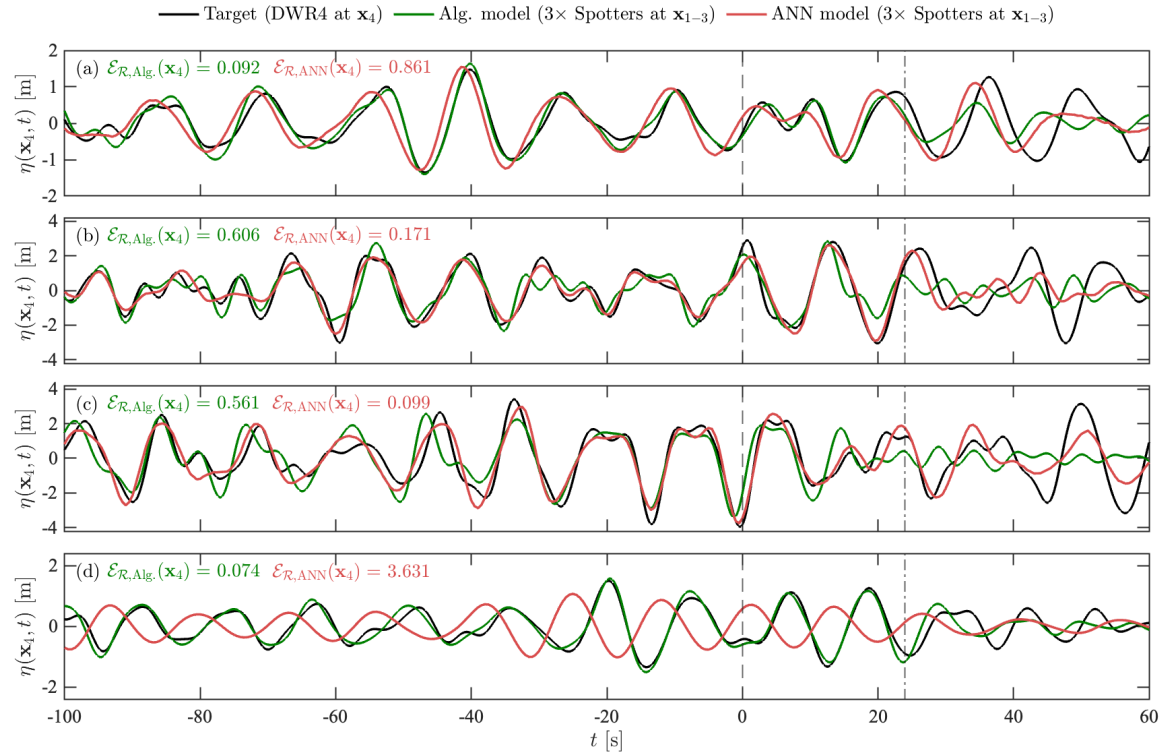

Fig. 9. Time series predictions corresponding to the array configurations in Fig. 8. The averaged errors are calculated over the prediction horizon $t \in [0, 24]$ s (within the vertical dashed lines).

investigate this further, we select 4 cases on different days (marked as vertical dash-dotted lines in Fig. 7), where there are significant discrepancies in prediction error between the models.

The positions and bulk parameters of selected cases are presented in Fig. 8, and their corresponding prediction results are shown in Fig. 9. In cases (a) and (d), the mean wave directions $\overline{\theta}$ and spreading angles σ_θ are relatively smaller compared to cases (b) and (c). Additionally, the peak period T_p and wavelength λ_p are larger, which indicates both cases have longer waves, resulting in less misalignment at the prediction location. Hence, the predictions are expected to be more accurate for the algebraic model as demonstrated in Fig. 9(a) and (d). In contrast, case (c) has the largest separation angle $\overline{\theta} - \theta_A = 18°$, RMS spreading angle $\sigma_\theta = 28.9°$ and shorter wave period. Therefore, it is less predictable for the algebraic model, as shown in Fig. 9(c). In contrast, the ANN model achieves better accuracy and a longer prediction horizon for cases (b) and (c). These prediction results are expected and consistent with our previous analysis of synthetic data, as the ANN model has a wider coverage in mean wave directions and better alignment in wave spreading than the algebraic model. However, it is shown that the ANN prediction result of case (a) has approximately a 2 s time difference to target waves, and the prediction is out-of-phase for case (d), resulting in large error values. The observed phase difference is primarily caused by the displacement of the buoys from their long-term averaged positions. The ANN model assumes fixed positions of the buoys whereas the algebraic model

takes into account the current positions of the buoys based on their GPS coordinates.

Fig. 10(a) depicts the positions of the three Spotters and the DWR4 corresponding to Fig. 9(a). The grey dots indicate the positions of the Spotters and DWR4 during training, while the black dots indicate their positions during testing, both with 1-minute intervals between the dots. It should be noted that DWR4 recorded data every 2^{nd} and 10^{th} minute, instead of every 10^{th} minute as per the manual [22], resulting in the relatively coarse interpolation of the positions. As shown in Fig. 10(b), the positions of DWR4 during testing moved away from its during training. Since the ANN model is a purely data-driven method that relies solely on the input time histories of the motions over the faster wave frequencies, it assumes the prediction distance (distance from the Spotter array to the DWR4) during testing would be similar to that during training.

As shown in Fig. 11, the error increases gradually when the DWR4 deviates from its training positions, and conversely, the error decreases as the DWR4 returned to its training positions. This observation further demonstrated that the error is primarily dominated by the change of positions, particularly along the mean wave direction. Similarly, the error of Fig. 9(d) is caused by a larger moving distance, with the DWR4 moving from approximately 250 m to 350 m along the North within training and testing positions. Hence, it is important to incorporate the position information into the ANN model. One possible solution to this issue is calculating the phase difference based on the moving distance. However, obtaining accurate phase shift correction is challenging due to the roughly estimated prediction distance interpreted from the ANN model. Moreover, a reduction in accuracy on troughs and peaks can be observed after the phase correction when the moving distance becomes significant. In contrast, the algebraic model inputs the mean buoy positions within the measurement time. Hence, the prediction accuracy is much less affected by the slow-scale motion. We also note that previous work [23] on DWR4 records from this location shows that the wind has a significant effect on the motion of the buoy within its watch circle.

Another limitation of the ANN model is the need for the past 6 hours of training data, periodically updated with recent data to adapt to changing wave conditions and buoy positions, which could delay the initial prediction during practical applications. In contrast, the algebraic model only requires 204.8 s of past time histories for prediction. It is worth noting that it is possible to train an ANN model with more historical data (i.e., a year of data from Sandpatch) with varying positions. However, if the new data introduces dissimilarities, in particular, the variation in positions that the model cannot generalize well, its performance will be impaired considerably.

It should also be noted that a decrease in accuracy due to the change in bulk parameters, such as H_s and T_p, is minor compared to the change in positions because the difference in these parameters is relatively small between the validation (past 30 min) and testing

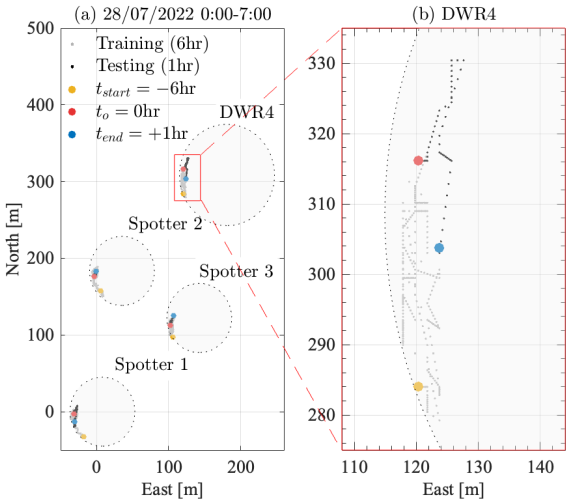

Fig. 10. Array positions of field data from 0:00-7:00 on July 28, with a time interval of 1 minute between the small dots. Yellow dots indicate the starting position of training data, red dots indicate the starting position of testing and blue dots indicate the last position of testing. (a) Spotters and DWR4 positions over the duration. (b) Close-up view of the red rectangular box for DWR4.

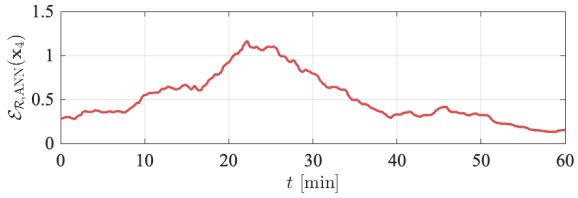

Fig. 11. Averaged prediction error of ANN model from 6:00-7:00 on July 28.

data (1 hour into the future). Additionally, the model has been generalized well based on the different sea-state combinations in the past 6 hours.

V. Conclusion

This study compared a machine learning method based on an Artificial Neural Network (ANN) model to a physics-based algebraic model for phase-resolved wave prediction. The models predict surface waves at the downwave location of a Datawell Waverider-4 (DWR4) using past information on ocean surface elevation and x, y displacements measured by three Spotters at upwave locations. We first analyze the prediction performance of the models using synthetic short-crested waves generated with average wave parameters for the Albany location under study and a fixed array of ideal wave buoys. The results show that the ANN model achieves better prediction accuracy and horizon with wider coverage of mean wave direction $\overline{\theta}$ and larger spreading angles σ_θ compared to the algebraic model.

We further compared the prediction schemes of the models using field data measured using wave buoys deployed in the Southern Ocean near Sandpatch, Albany, Western Australia. We have demonstrated that the ANN model achieves better prediction results when the mean wave direction and spreading angle are large, consistent with our observation using syn-

thetic data. However, the generalization capability of the ANN model is limited by the change in overall buoy positions over slow times scales compared to the waves, leading to phase offsets in the prediction. In contrast, the algebraic model can partly account for buoys moving distance in the positions of the wave buoys. Notably, the error of the algebraic model strongly depends on the mean wave directions and spreading angles, evidenced by a strong correlation.

Overall, the results suggest that the algebraic model is more robust for practical adaptations in sea states with moderate spreading sizes. For larger wave separation and spreading angles, the ANN model shows promise as an alternative method to improve prediction accuracy. It is important to note, however, that further research is needed to incorporate the positions into the ANN model to correct the phases. A possible approach could be to use a physics-informed neural network that accounts for changes in buoy locations and learns how waves propagate through space and time based on physical principles. Such a model would likely result in more accurate predictions and would be worth exploring in future studies.

ACKNOWLEDGEMENT

This research is supported by the ARC ITRH for Transforming Energy Infrastructure through Digital Engineering (TIDE, http://TIDE.edu.au) which is led by The University of Western Australia, delivered with The University of Wollongong and several other Australian and International research partners, and funded by the Australian Research Council, INPEX Operations Australia, Shell Australia, Woodside Energy, Fugro Australia Marine, Wood Group Kenny Australia, RPS Group, Bureau Veritas and Lloyd's Register Global Technology (Grant No. IH200100009).

REFERENCES

[1] J. Hals, T. Bjarte-Larsson, and J. Falnes, "Optimum reactive control and control by latching of a wave-absorbing semisubmerged heaving sphere," in *International Conference on Offshore Mechanics and Arctic Engineering*, vol. 36142, 2002, pp. 415–423.

[2] J. Falnes, "Optimum control of oscillation of wave-energy converters," in *The Eleventh International Offshore and Polar Engineering Conference*, vol. 12, no. 2, 2001, pp. 147–155.

[3] J. C. C. Henriques, L. M. C. Gato, A. F. d. O. Falcão, E. Robles, and F.-X. Faÿ, "Latching control of a floating oscillating-water-column wave energy converter," *Renewable Energy*, vol. 90, pp. 229–241, 2016.

[4] T. Hlophe, P. H. Taylor, A. Kurniawan, J. Orszaghova, and H. Wolgamot, "Phase-resolved wave prediction in highly spread seas using optimised arrays of buoys," *Applied Ocean Research*, vol. 130, p. 103435, 2023.

[5] J. Zhang, J. Yang, J. Wen, I. Prislin, and K. Hong, "Deterministic wave model for short-crested ocean waves: Part I. Theory and numerical scheme," *Applied Ocean Research*, vol. 21, no. 4, pp. 167–188, 1999.

[6] A. Fisher, J. Thomson, and M. Schwendeman, "Rapid deterministic wave prediction using a sparse array of buoys," *Ocean Engineering*, vol. 228, p. 108871, 2021.

[7] T. T. Janssen, A. R. Van Dongeren, and C. Kuiper, "Phase resolving analysis of multidirectional wave trains," in *Ocean Wave Measurement and Analysis (2001)*, 2002, pp. 377–387.

[8] Y. Z. Law, H. Santo, K. Y. Lim, and E. S. Chan, "Deterministic wave prediction for unidirectional sea-states in real-time using Artificial Neural Network," *Ocean Engineering*, vol. 195, p. 106722, 2020.

[9] W. Duan, X. Ma, L. Huang, Y. Liu, and S. Duan, "Phase-resolved wave prediction model for long-crest waves based on machine learning," *Computer Methods in Applied Mechanics and Engineering*, vol. 372, p. 113350, 2020.

[10] J. Zhang, X. Zhao, S. Jin, and D. Greaves, "Phase-resolved real-time ocean wave prediction with quantified uncertainty based on variational Bayesian machine learning," *Applied Energy*, vol. 324, p. 119711, 2022.

[11] T. Hlophe, H. Wolgamot, P. H. Taylor, A. Kurniawan, J. Orszaghova, and S. Draper, "Wave-by-wave prediction in weakly nonlinear and narrowly spread seas using fixed-point surface-elevation time histories," *Applied Ocean Research*, vol. 122, p. 103112, 2022.

[12] M. J. Tucker, P. G. Challenor, and D. J. T. Carter, "Numerical simulation of a random sea: A common error and its effect upon wave group statistics," *Applied Ocean Research*, vol. 6, no. 2, pp. 118–122, 1984.

[13] T. Hlophe, P. H. Taylor, A. Kurniawan, J. Orszaghova, and H. Wolgamot, "Optimised wave-by-wave prediction of spread waves: Comparison with field data," in *ASME 2023 42nd International Conference on Offshore Mechanics and Arctic Engineering*. American Society of Mechanical Engineers Digital Collection, 2023 (Accepted).

[14] G. Lindgren, "Some properties of a normal process near a local maximum," *The Annals of Mathematical Statistics*, vol. 41, no. 6, pp. 1870–1883, 1970. [Online]. Available: http://www.jstor.org/stable/2240325

[15] I. Goodfellow, Y. Bengio, and A. Courville, *Deep learning*. MIT Press, 2016.

[16] J. Chen, W. Zhao, I. A. Milne, D. Gunawan, and P. H. Taylor, "Weakly nonlinear surface wave prediction using a data-driven method with the help of physical understanding," in *ASME 2023 42nd International Conference on Offshore Mechanics and Arctic Engineering*. American Society of Mechanical Engineers Digital Collection, 2023 (Accepted).

[17] K. Jarrett, K. Kavukcuoglu, M. Ranzato, and Y. LeCun, "What is the best multi-stage architecture for object recognition?" in *International Conference on Computer Vision*. IEEE, 2009, pp. 2146–2153.

[18] D. P. Kingma and J. Ba, "Adam: A method for stochastic optimization," in *International Conference on Learning Representations, arXiv:1412.6980*, 2014.

[19] F. Chollet *et al.*, "Keras: Deep learning library for Theano and Tensorflow," 2015. [Online]. Available: https://github.com/fchollet/keras

[20] M. Abadi *et al.*, "Tensorflow: Large-scale machine learning on heterogeneous distributed systems," 2016. [Online]. Available: https://www.tensorflow.org

[21] A. J. Kuik, G. P. Van Vledder, and L. H. Holthuijsen, "A method for the routine analysis of pitch-and-roll buoy wave data," *Journal of physical oceanography*, vol. 18, no. 7, pp. 1020–1034, 1988.

[22] Datawell BV, "Datawell Waverider-4 (DWR4) manual," 2023. [Online]. Available: https://datawell.nl/wp-content/uploads/2023/02/datawell_manual_dwr4_2023-02-15.pdf

[23] A. Kurniawan, P. H. Taylor, J. Orszaghova, H. Wolgamot, and J. Hansen, "Measuring a rogue? an investigation into an apparent giant wave," *Journal of Atmospheric and Oceanic Technology*, vol. 39, no. 8, pp. 1129–1147, 2022.